# Effect of Amorphous-Crystalline Phase Transition on Superlubric Sliding

Ebru Cihan,[1,2] Dirk Dietzel,[1,3,*] Benedykt R. Jany,[4] and André Schirmeisen[1,3]
[1]Institute of Applied Physics, Justus-Liebig-Universität Giessen, 35392 Giessen, Germany
[2]Institute for Materials Science and Max Bergmann Center for Biomaterials, TU Dresden, 01069 Dresden, Germany
[3]Center for Materials Research, Justus-Liebig-Universität Giessen, 35392 Giessen, Germany
[4]Marian Smoluchowski Institute of Physics, Faculty of Physics, Astronomy and Applied Computer Science, Jagiellonian University, 30348 Krakow, Poland

(Received 23 May 2022; accepted 26 January 2023; published 24 March 2023)

Structural superlubricity describes the state of greatly reduced friction between incommensurate atomically flat surfaces. Theory predicts that, in the superlubric state, the remaining friction sensitively depends on the exact structural configuration. In particular the friction of amorphous and crystalline structures for, otherwise, identical interfaces should be markedly different. Here, we measure friction of antimony nanoparticles on graphite as a function of temperature between 300 and 750 K. We observe a characteristic change of friction when passing the amorphous-crystalline phase transition above 420 K, which shows irreversibility upon cooling. The friction data is modeled with a combination of an area scaling law and a Prandtl-Tomlinson type temperature activation. We find that the characteristic scaling factor $\gamma$, which is a fingerprint of the structural state of the interface, is reduced by 20% when passing the phase transition. This validates the concept that structural superlubricity is determined by the effectiveness of atomic force canceling processes.

DOI: 10.1103/PhysRevLett.130.126205

The tribological phenomenon of structural superlubricity is characterized by ultralow friction between atomically flat and incommensurate surfaces that can be achieved through collective force cancellations during relative motion. Understanding the mechanisms and, especially, limitations that determine the effectiveness of force cancellations is not only of fundamental interest in nanotribology, but also relevant to design superlubric interfaces for technical applications.

Consequently, a growing number of studies have analyzed superlubricity and the influence of different key factors both in theory and by nanoscale experiments [1–5]. In particular, interface contamination [6–12], interface size, shape, and orientation [13–19], interface relaxations and (local) commensurability [20–26], as well as the role of crystalline structure [13,14,27] have been considered as important factors for the efficiency of superlubric force cancellations. Concerning the crystalline structure, current models predict that well-ordered surfaces allow for more comprehensive force cancellations as compared to amorphous interfaces, where the statistical positioning of the interface atoms limits the potential for superlubricity [28]. Despite this fundamental character of this paradigm of superlubricity, a direct experimental verification is still lacking.

Previous experiments have linked amorphous and crystalline interfaces with different contact area scaling relations for gold and antimony particles [13]. However, open questions remained about the influence of the chemical nature of these two materials. A direct transition of the interface structure without modifying the chemical nature of the surfaces, would give direct verification of the atomic origins of structural superlubricity.

Here, we are analyzing Sb-nanoparticles on HOPG for temperatures between 300 and 750 K. Sb nanoparticles on HOPG are known to exhibit an irreversible and controllable transition from amorphous to crystalline structure induced in the antimony particles by heating to temperatures of approximately 130°–170 °C [29–32]. Indeed, we find a clear fingerprint of this transition in our atomic force microscopy (AFM) nanomanipulation experiments. Comparison of friction levels at 300 K before and after heating allows us to quantify the change in superlubricity, which are compared to different concepts of interface changes. Ultimately, the observed friction changes of approximately 50% suggest a scenario where the superlubric friction reduction is limited by remaining structural irregularities such as the particle border and grain boundaries at a polycrystalline interface.

Friction between the nanoparticles and the substrate was measured using a nanomanipulation approach, based on detecting the torsional signal from the cantilever when the AFM tip pushes the particle across the substrate [3,6,11,13,27]. All nanoparticle-samples were prepared by thermal deposition of antimony onto highly oriented pyrolytic graphite. The HOPG was freshly cleaved in air before transfer to the ultrahigh vacuum (UHV) chamber with a base pressure of $5 \times 10^{-10}$ mbar. To remove adsorbates, the HOPG was heated to 200 °C for 2 h.

 

Evaporation of antimony then took place at deposition temperatures of 400 °C for 5–10 min (see [27]). This procedure resulted in well-defined nanoparticles with atomically flat interfaces between particles and substrate [6,33,34]. Under these preparation conditions the Sb nanoparticles are amorphous, which is further validated by their size and compact shape [13,35].

After preparation and without breaking the vacuum, the samples were transferred to the UHV-AFM (VT-AFM, Omicron Nanotechnology GmbH). All nanomanipulation experiments have been performed as a three-step process: (i) To avoid scanning-induced movement of nanoparticles, the surface was first imaged in noncontact mode and a nanoparticle for manipulation was chosen [Fig. 1(a), top]. (ii) The AFM tip was placed next to the nanoparticle and the system was switched to contact mode. The particle was then pushed perpendicular to the long cantilever axis, while the lateral force signal $F_L$ was recorded [Fig. 1(b)]. (iii) The particle displacement was verified by a control image using noncontact mode [Fig. 1(a), bottom].

The effective particle friction was calculated from the difference of the pushing force during sliding and the lateral force experienced by the AFM tip on the HOPG before reaching the nanoparticle [Fig. 1(b)]. Lateral force calibration was based on the method by Bilas *et al.* [36]. We used typical normal loads of $F_n = 75$ nN in the first set of experiments and 101 nN in the second, with a constant sliding velocity of 417 nm/s. The contact area $A$ of each particle was determined from AFM topography images.

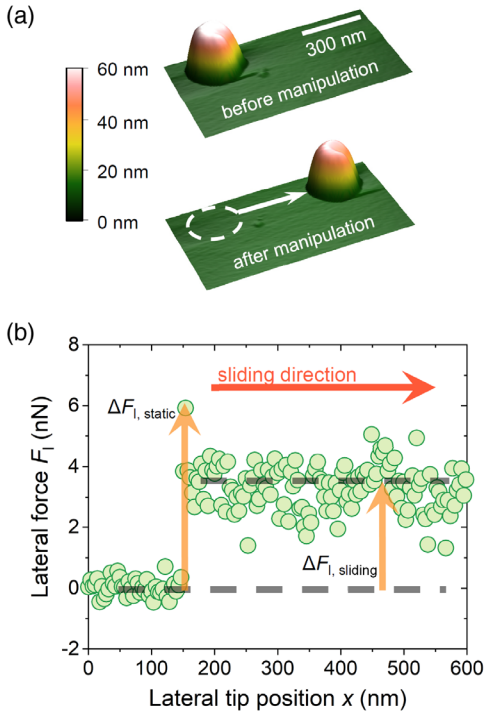


FIG. 1. Lateral manipulation of an antimony nanoparticle on graphite. (a) Top: AFM topography image before manipulation. Bottom: Topography image after manipulation. (b) Lateral force signal along the path of manipulation. The AFM tip reaches the nanoparticle at about $x = 150$ nm and the lateral force signal increases to $\Delta F_{l,\mathrm{static}}$ before $\Delta F_{l,\mathrm{sliding}}$ then corresponds to the sliding friction of the nanoparticle.

The first set of experiments was performed for a group of three nanoparticles of similar contact area and at temperatures between 300 and 750 K. Within this range, the temperature was progressively increased in steps of 50 K resulting in friction values for ten different temperatures. To ensure that the exact same particles were measured at each temperature, thermal drift during temperature changes was compensated based on continuous imaging of the relevant sample area.

Figure 2 displays a similar temperature dependence for all three particles, where three different regimes can be

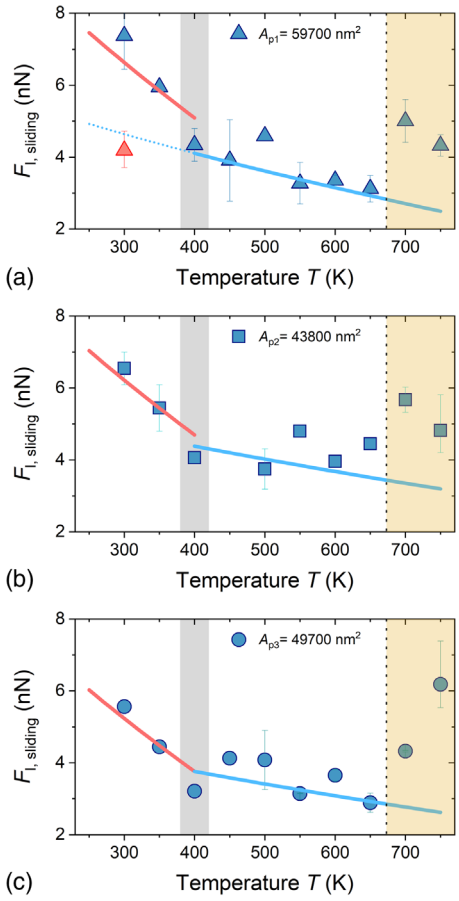


FIG. 2. (a)–(c) Temperature dependence of sliding friction measured for three different nanoparticles for continuously increasing temperatures between 300 and 750 K (blue symbols). The red data point in (a) was recorded after cooling particle 1 from 750 back to 300 K. For increasing temperatures below 700 K the temperature dependence can be divided into two regimes as indicated by the theoretical curves based on thermally activated stick slip (continuous lines). The transition corresponds to the typical temperature range for structural phase transitions of nanoscale antimony as indicated by the grey background color. In addition, a high temperature regime with increased friction emerges once the sample temperature exceeds 400 °C.

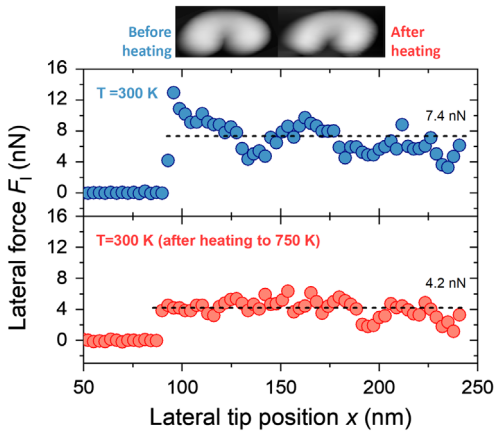


FIG. 3. Friction forces measured during manipulation of nanoparticle 1 [$A = 59\,700$ nm$^2$, Fig. 2(a)] at 300 K before and after heating. A significant reduction in friction by a factor of 1.76 is found. In addition, the AFM-topography images (top) verify that particle size and shape have not changed during exposure to high temperatures. In particular, no significant evaporation of antimony occurred.

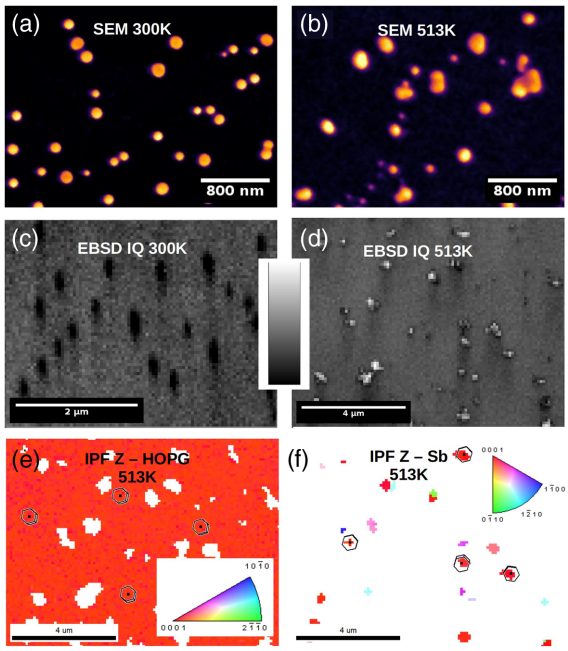


FIG. 4. SEM and EBSD analysis of Sb particles on HOPG. (a), (b) SEM surface morphology of the unheated sample (a) and the sample heated to 513 K (b). (c),(d) SEM EBSD IQ maps of the unheated sample (c) and the sample heated to 513 K (d). (e),(f) EBSD inverse pole figure maps ($Z$ out of plane) for HOPG (e) and the heated Sb particles (f). The orientation of hexagonal unit cells is shown for selected points.

distinguished. Over the whole temperature range, sliding friction varies by a factor of 3.3 for the first nanoparticle, 2.6 for the second nanoparticle, and 2.8 for the third nanoparticle. The red data point in Fig. 2(a) refers to the sliding friction of particle 1 ($A = 59\,700$ nm$^2$) when it cooled back to 300 K after exposure to high temperatures. This documents a friction reduction by a factor of 1.76. Figure 3 shows the friction traces recorded during manipulation of this nanoparticle at 300 K before and after the high temperature treatment. This result suggests that a temperature induced irreversible change of the interface has occurred. While such changes can be ruled out for HOPG, phase transitions of antimony are well-known occurrences in nanoscale systems [29–31,37–45]. The crystalline structure depends on the system size, and transitions from amorphous to crystalline structure can occur once a critical film thickness or particle size is exceeded [34,42,46,47]. At the same time, temperature also plays an important role for phase transitions in nanoscale antimony structures [37,40], and sufficient temperature can induce a transition from amorphous to crystalline state in thin films [41,43], nanowires [29,30], or nanoparticles [31,32] with typical transition temperatures around 400–420 K.

To verify the occurrence of a temperature induced phase transition for our nanoparticles, we prepared two new samples, one of which was heated to 513 K for 5 h. Both samples have then been analyzed by SEM EBSD (scanning electron microscopy electron backscatter diffraction, see, also, the Supplemental Material [48]). The SEM images [Figs. 4(a) and 4(b)] illustrate the general topography, while Figs. 4(c) and 4(d) show standard EBSD IQ (image quality) maps. In these maps, the brightness of each pixel represents a relative measure for the diffraction pattern quality that is calculated from local EBSD patterns as average of the peaks in the Hough Transform space [49,50]. Comparing the crystalline HOPG substrate with the nanoparticles, we find that the intensity of the HOPG far exceeds that of the unheated particles, which appear as dark spots in Fig. 4(c) due to their amorphous structure. On contrary, the heated nanoparticles [Fig. 4(d)] appear as bright spots since their crystalline structure and high mass number result in high IQ. Additionally, the detailed diffraction patterns (see Supplemental Material [48]) also corroborate the structural difference.

A more detailed analysis of the heated nanoparticles was done by EBSD inverse pole figures (IPFs) ($Z$ out of plane) studies [51], which show crystallographic orientations by color-coded maps [Figs. 4(e) and 4(f)]. The IPF map on HOPG confirms the (0001) orientation [Fig. 4(e)]. Figure 4(f) then shows the orientation distribution for different nanoparticles. In the majority of cases, we find (0001) orientation, which means that sliding mainly occurs at the (0001)Sb//(0001)HOPG interface (cf. Supplemental Material [48]).

Based on the EBSD analysis, we assign the change in friction in our Sb sliding experiments to a thermally triggered phase transition. The observed transition temperature at about 400 K (Fig. 2), is consistent with the above findings. In addition, the absolute friction values for the amorphous state are well in line with previous results for Sb

particles on HOPG in the superlubric regime, where a link between particle friction and diffusion energy barrier was possible [13].

Next, we model the experimental friction $F_L$ as a thermally activated Prandtl-Tomlinson process [52–55]

$$F_L(T) = F_c - \left[\beta k_B T ln\left(\frac{v_c}{v}\right)\right]^{2/3} \quad (1)$$

with a critical velocity $v_c$ of

$$v_c = (2f_0\beta k_b T)/(3c_{\text{eff}}\sqrt{F_c}). \quad (2)$$

Here, $f_0$ is the attempt frequency, $c_{\text{eff}}$ the effective contact stiffness and the factor $\beta$ is a measure for the curvature of the potential energy corrugation.

The key parameter for describing the different superlubric states for crystalline and amorphous particles is the effective energy barrier. For an ideal sinusoidal energy landscape the effective energy barrier $E_0$ is linked to the critical force $F_c$ by $\beta_{\text{sin}} = (3\pi F_c)/(2\sqrt{2}a)$ and $F_c = \pi E_0/a$ with $a$ as the lattice constant of the substrate. Since superlubric force canceling for an amorphous interface is less effective than for a crystalline interface, we expect a lower energy barrier for the crystalline state.

A number of experimental works using friction force microscopy (FFM) [56] indicated a significant deviation between $\beta$ and $\beta_{\text{sin}}$. Factors of approximately 2–6 have been found for the ratio $\delta = \beta/\beta_{\text{sin}}$ during velocity and temperature dependent FFM on mica or HOPG [54,55]. Therefore, we treat $\beta$ as an additional fit parameter. We find that the phase transition is not only reflected in the critical forces $F_c$ but also in $\beta$ (Table I). This emphasizes the different mechanisms of force cancellation in the two phases. The critical forces $F_c$ between the temperature regimes differ by a factor of 2. Extrapolation of the crystalline theoretical curve for particle 1 also yields a good approximation for the friction value measured at 300 K after heating [Fig. 2(a)]. Finally, we look at the experimental observation of increasing friction for the highest temperatures ($T \geq 700$ K), which might be tentatively linked to increased interface relaxations when measuring at temperatures suitable for sublimation and approaching the solid-liquid transition at 630 °C.

TABLE I. Parameters to calculate the theoretical curves in Fig. 2. The table shows only varying parameters. Additionally, $a = 2.5$ Å and $f_0/c_{\text{eff}} = 1.4 \times 10^{11}$ m/Ns were used for all temperatures and particles.

| Particle | $T$ range | $F_c$/N | $\delta$ |
|---|---|---|---|
| 1 | Low | $13.5 \times 10^{-9}$ | 5 |
| 1 | High | $7 \times 10^{-9}$ | 1.5 |
| 2 | Low | $13 \times 10^{-9}$ | 5 |
| 2 | High | $6.5 \times 10^{-9}$ | 1 |
| 3 | Low | $11.8 \times 10^{-9}$ | 5 |
| 3 | High | $5.8 \times 10^{-9}$ | 1 |

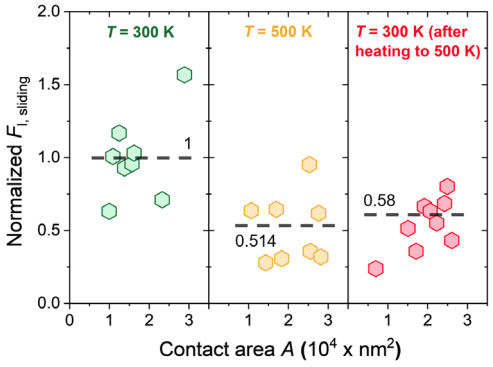


FIG. 5. Irreversible friction changes for Sb nanoparticles after heating to 500 K. The friction values were obtained at three different temperatures from nanomanipulation experiments for three different groups of nanoparticles of similar size. Left: friction measurements at 300 K, Middle: friction measurements after heating the sample to 500 K, Right: friction measurements at 300 K after the sample was cooled down again. After heating, the nanoparticle friction is reduced by a factor of approximately 2.

To further validate the irreversible phase transition, we performed manipulation experiments on a new sample for three different random groups of nanoparticles of similar size. First, the friction of a set of eight nanoparticles was analyzed at 300 K prior to any heating of the sample (Fig. 5, left). After that, the sample was heated to 500 K, and a second set of eight nanoparticles was analyzed (Fig. 5, middle). Finally, sliding friction was measured for a third set of nine nanoparticles after the sample cooled back down to 300 K (Fig. 5, right).

The results confirm the observations from Fig. 2(a). At low temperature, friction is highest and is reduced roughly by a factor of 2 when heating to 500 K. This friction change is then found to be irreversible, since the same level of friction is measured after cooling back to room temperature. In addition, the absolute friction values also compare well to Fig. 2.

Next, we want to correlate the relative friction changes in Fig. 5 with the superlubricity model predictions from "scaling law" [11,13,15,28]. In this concept, the effective energy barrier for sliding $\Delta E$ is linked to the number of interface atoms $N$ by a power law as $\Delta E = \Delta E_0 \times N^\gamma$, where $\Delta E_0$ represents the single-atom energy barrier. As a first approximation, we assume that the sliding friction values are directly proportional to the energy barrier $\Delta E$ and can be described as $F_{\text{sliding}} = F_0 \times N^\gamma$ with $F_0$ as the single atom friction.

In both cases, $\gamma$ is a characteristic scaling factor that sensitively depends on parameters like crystalline structure, shape, or relative orientation between substrate and slider [13,14,17]. For amorphous sliders, the scaling factor

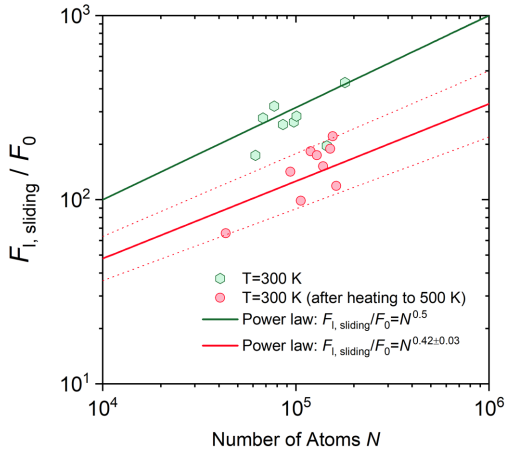


FIG. 6. Normalized sliding friction as a function of the number of antimony atoms at the interface measured for 2 ensembles of nanoparticles at 300 K before (green hexagons) and after (red circles) heating the sample to 500 K. The straight lines represent the scaling of friction vs the atom number for the two cases. The friction data has been normalized by the single atom friction of antimony on HOPG which, in turn, was derived from fitting $F_{l,\mathrm{sliding}} = F_0 N^{0.5}$ to the dataset analyzed before heating. From the dotted lines, the error of $\gamma'$ can be estimated.

is $\gamma = 0.5$ independent of shape and relative orientation. Thus, we have fitted the data of Fig. 5 obtained at 300 K before heating with a fixed scaling factor $\gamma = 0.5$, yielding the single atom friction value $F_0$. This allows us to normalize the data of Fig. 5 obtained at 300 K before and after heating by $F_0$. A fit to the normalized friction data after the heating cycle results in a scaling factor of $\gamma' = 0.42 \pm 0.03$, accounting for the temperature induced phase transition (Fig. 6). (Please note, that the fitting result is mostly determined by the absolute changes in friction.) By further considering a potential influence of $\beta$ on the friction vs area scaling, an even reduced value of $\gamma' = 0.371$ can be estimated (see Supplemental Material [48]).

The scaling analysis validates the idea that superlubric force cancellations become more efficient after the phase transition from amorphous to crystalline. The round shape of the particles allows a theoretical minimum of $\gamma = 0.25$ [13,17]. The observed reduction of $\gamma = 0.5$ to $\gamma' \approx 0.37$–$0.42$ here might appear moderate but already compares well to previous experimental results, where a value of $\gamma = 0.33$ was found for crystalline gold nanoparticles sliding on HOPG. In our case, disordered grain boundaries and random grain orientations as well as defects might counteract the force cancellation process, which can increase friction and, thus, $\gamma$.

In summary, we find a characteristic and irreversible change in the sliding friction behavior of Sb nanoparticles when undergoing a structural phase transition from amorphous to crystalline. These results highlight the general importance of the atomic structure at the sliding interface in the superlubric regime. Experiments on idealized model systems like this help our understanding of how forces of each atom at the sliding interface act synergistically to enhance or cancel their contributions. At the same time, applications of superlubricity are rapidly evolving [57–60], requiring a thorough knowledge of the underlying mechanisms.

D. D. and A. S. acknowledge financial support provided by the Deutsche Forschungsgemeinschaft (DFG) (Projects No. DI917/6-1, No. DI917/7-1, No. DI917/8-1, and No. SCHI619/10-1). This research was supported in part by the Excellence Initiative—Research University Program at the Jagiellonian University in Krakow.

*dirk.dietzel@ap.physik.uni-giessen.de

[1] W. Zhai and K. Zhou, Nanomaterials in superlubricity, Adv. Funct. Mater. **29**, 1806395 (2019).
[2] M. Z. Baykara, M. R. Vazirisereshk, and A. Martini, Emerging superlubricity: A review of the state of the art and perspectives on future research, Appl. Phys. Rev. **5**, 041102 (2018).
[3] D. Dietzel, U. Schwarz, and A. Schirmeisen, Nanotribological studies using nanoparticle manipulation: Principles and application to structural lubricity, Friction **2**, 114 (2014).
[4] A. Vanossi, D. Dietzel, A. Schirmeisen, E. Meyer, R. Pawlak, T. Glatzel, M. Kisiel, S. Kawai, and N. Manini, Recent highlights in nanoscale and mesoscale friction, Beilstein J. Nanotechnol. **9**, 1995 (2018).
[5] Y. Song, C. Qu, M. Ma, and Q. Zheng, Structural superlubricity based on crystalline materials, Small **16**, 1903018 (2020).
[6] D. Dietzel, C. Ritter, T. Monninghoff, H. Fuchs, A. Schirmeisen, and U. Schwarz, Frictional Duality Observed during Nanoparticle Sliding, Phys. Rev. Lett. **101**, 125505 (2008).
[7] D. Dietzel, T. Monninghoff, C. Herding, M. Feldmann, H. Fuchs, B. Stegemann, C. Ritter, U. Schwarz, and A. Schirmeisen, Frictional duality of metallic nanoparticles: Influence of particle morphology, orientation, and air exposure, Phys. Rev. B **82**, 035401 (2010).
[8] M. H. Müser, L. Wenning, and M. O. Robbins, Simple Microscopic Theory of Amontons's Laws for Static Friction, Phys. Rev. Lett. **86**, 1295 (2001).
[9] J. Brndiar, R. Turansky, D. Dietzel, A. Schirmeisen, and I. Stich, Understanding frictional duality and bi-duality: Sb-nanoparticles on HOPG, Nanotechnology **22**, 085704 (2011).
[10] H. Deng, M. Ma, Y. Song, Q. He, and Q. Zheng, Structural superlubricity in graphite flakes assembled under ambient conditions, Nanoscale **10**, 14314 (2018).
[11] E. Cihan, S. Ipek, E. Durgun, and M. Z. Baykara, Structural lubricity under ambient conditions, Nat. Commun. **7**, 12055 (2016).
[12] A. Özogul, S. Ipek, E. Durgun, and M. Z. Baykara, Structural superlubricity of platinum on graphite under ambient conditions: The effects of chemistry and geometry, Appl. Phys. Lett. **111**, 211602 (2017).

[13] D. Dietzel, M. Feldmann, U. D. Schwarz, H. Fuchs, and A. Schirmeisen, Scaling Laws of Structural Lubricity, Phys. Rev. Lett. **111**, 235502 (2013).
[14] A. S. de Wijn, (In)commensurability, scaling, and multiplicity of friction in nanocrystals and application to gold nanocrystals on graphite, Phys. Rev. B **86**, 085429 (2012).
[15] E. Koren, E. Lörtscher, C. Rawlings, A. W. Knoll, and U. Duerig, Adhesion and friction in mesoscopic graphite contacts, Science **348**, 679 (2015).
[16] S. Kawai, A. Benassi, E. Gnecco, H. Söde, R. Pawlak, X. Feng, K. Müllen, D. Passerone, C. A. Pignedoli, P. Ruffieux, R. Fasel, and E. Meyer, Superlubricity of graphene nanoribbons on gold surfaces, Science **351**, 957 (2016).
[17] D. Dietzel, A. de Wijn, M. Vorholzer, and A. Schirmeisen, Friction fluctuations of gold nanoparticles in the superlubric regime, Nanotechnology **29**, 155702 (2018).
[18] Q. Zheng, B. Jiang, S. Liu, J. Zhu, Q. Jiang, Y. Weng, L. Lu, S. Wang, Q. Xue, and L. Peng, Self-Retracting Motion of Graphite Microflakes, Phys. Rev. Lett. **100**, 067205 (2008).
[19] Z. Liu, J. Yang, F. Grey, J. Z. Liu, Y. Liu, Y. Wang, Y. Yang, Y. Cheng, and Q. Zheng, Observation of Microscale Superlubricity in Graphite, Phys. Rev. Lett. **108**, 205503 (2012).
[20] D. Dietzel, J. Brndiar, I. Sttich, and A. Schirmeisen, Limitations of structural superlubricity: Chemical bonds versus contact size, ACS Nano **11**, 7642 (2017).
[21] M. Feldmann, D. Dietzel, H. Fuchs, and A. Schirmeisen, Influence of Contact Aging on Nanoparticle Friction Kinetics, Phys. Rev. Lett. **112**, 155503 (2014).
[22] M. Feldmann, D. Dietzel, A. Tekiel, J. Topple, P. Grutter, and A. Schirmeisen, Universal Aging Mechanism for Static and Sliding Friction of Metallic Nanoparticles, Phys. Rev. Lett. **117**, 025502 (2016).
[23] T. A. Sharp, L. Pastewka, and M. O. Robbins, Elasticity limits structural superlubricity in large contacts, Phys. Rev. B **93**, 121402(R) (2016).
[24] A. Vanossi, N. Manini, and E. Tosatti, Static and dynamic friction in sliding colloidal monolayers, Proc. Natl. Acad. Sci. U.S.A. **109**, 16429 (2012).
[25] T. Bohlein, J. Mikhael, and C. Bechinger, Observation of kinks and antikinks in colloidal monolayers driven across ordered surfaces, Nat. Mater. **11**, 126 (2012).
[26] A. V. Khomenko, N. V. Prodanov, and B. N. J. Persson, Atomistic modelling of friction of Cu and Au nanoparticles adsorbed on graphene, Condens. Matter Phys. **16**, 33401 (2013).
[27] F. Hartmuth, D. Dietzel, A. de Wijn, and A. Schirmeisen, Friction vs area scaling of superlubric NaCl-particles on graphite, Lubricants **7**, 66 (2019).
[28] M. H. Mueser, Theoretical aspects of superlubricity, in *Fundamentals of Friction and Wear* (Springer, New York, 2007), pp. 177–199.
[29] C. Schoendorfer, A. Lugstein, L. Bischoff, Y. J. Hyun, P. Pongratz, and E. Bertagnolli, FIB induced growth of antimony nanowires, Microelectron. Eng. **84**, 1440 (2007).
[30] M. Barati, J. C. L. Chow, P. K. Ummat, and W. R. Datars, Temperature dependence of the resistance of antimony nanowire arrays, J. Phys. Condens. Matter **13**, 2955 (2001).
[31] N. Kaiser, H. Müller, and C. Gloede, Influence of the amorphous state on the structure of crystalline antimony films, Thin Solid Films **85**, 293 (1981).
[32] K. Tanaka, S. I. S. Iwama, and K. M. K. Mihama, Crystallization of nanometer-sized amorphous Sb particles formed by flowing gas evaporation technique, Jpn. J. Appl. Phys. **37**, L669 (1998).
[33] B. Kaiser, B. Stegemann, H. Kaukel, and K. Rademann, Instabilities and pattern formation during the self-organized growth of nanoparticles on graphite, Surf. Sci. **496**, L18 (2002).
[34] B. Stegemann, C. Ritter, B. Kaiser, and K. Rademann, Crystallization of antimony nanoparticles: Pattern formation and fractal growth, J. Phys. Chem. B **108**, 14292 (2004).
[35] C. Ritter, M. Z. Baykara, B. Stegemann, M. Heyde, K. Rademann, J. Schroers, and U. D. Schwarz, Nonuniform friction-area dependency for antimony oxide surfaces sliding on graphite, Phys. Rev. B **88**, 045422 (2013).
[36] P. Bilas, L. Romana, B. Kraus, Y. Bercion, and J. L. Mansot, Quantitative characterization of friction coefficient using lateral force microscope in the wearless regime, Rev. Sci. Instrum. **75**, 415 (2004).
[37] N. Kaiser, Crystallization of amorphous antimony films, *Thin Solid Films* (1984), Vol. 116, p. 259–265, 10.1016/0040-6090(84)90445-0.
[38] D. Fausti, O. V. Misochko, and P. H. M. van Loosdrecht, Ultrafast photoinduced structure phase transition in antimony single crystals, Phys. Rev. B **80**, 161207(R) (2009).
[39] D. Krebs, S. Raoux, C. T. Rettner, G. W. Burr, M. Salinga, and M. Wuttig, Threshold field of phase change memory materials measured using phase change bridge devices, Appl. Phys. Lett. **95**, 082101 (2009).
[40] A. S. Rogachev, S. G. Vadchenko, and A. S. Shchukin, SHS reaction and explosive crystallization in thin films: Resemblance and distinction, Int. J. Self Propag. High Temp. Synth. **26**, 44 (2017).
[41] Z. Cheng, T. Milne, P. Salter, J. S. Kim, S. Humphrey, M. Booth, and H. Bhaskaran, Antimony thin films demonstrate programmable optical nonlinearity, Sci. Adv. **7**, eabd7097 (2021).
[42] H. Kirmse, B. Stegemann, W. Neumann, K. Rademann, and B. Kaiser, Size-dependent phase transition from amorphous to crystalline in antimony clusters on crystalline surfaces, Microsc. Microanal. **9**, 338 (2003).
[43] H. Zou, Y. Hu, X. Zhu, and Z. Song, Simultaneously high thermal stability and ultra-fast phase change speed based on samarium-doped antimony thin films, RSC Adv. **7**, 31110 (2017).
[44] A. Kinbara, M. Ohmura, and A. Kikuchi, Crystallization of amorphous antimony films, Thin Solid Films **34**, 37 (1976).
[45] S. G. Vadchenko, D. Y. Kovalev, A. S. Shchukin, and A. S. Rogachev, Crystallization of amorphous antimony at room temperature: Non-uniqueness of patterning route, Int. J. Self Propag. High Temp. Synth. **27**, 180 (2018).
[46] M. H. B. Stiddard, Thin films of antimony on metallic substrates: Crystallite orientation and critical thickness for the occurrence of the amorphous-crystalline phase transition, J. Mater. Sci. Lett. **4**, 1157 (1985).
[47] K. Maki, Changes in electrical resistivity during amorphous-crystalline phase transition of antimony films, Jpn. J. Appl. Phys. **13**, 649 (1974).
[48] See Supplemental Material at http://link.aps.org/supplemental/10.1103/PhysRevLett.130.126205 for further

information on the friction vs. contact area scaling and the EBSD results.

[49] K. Kunze, S. I. Wright, B. L. Adams, and D. J. Dingley, Advances in automatic EBSP single orientation measurements, Textures Microstruct. **20**, 41 (1993).

[50] S. I. Wright and M. M. Nowell, EBSD image quality mapping, Microsc. Microanal. **12**, 72 (2006).

[51] B. R. Jany, N. Gauquelin, T. Willhammar, M. Nikiel, K. H. W. van den Bos, A. Janas, K. Szajna, J. Verbeeck, S. Van Aert, G. Van Tendeloo, and F. Krok, Controlled growth of hexagonal gold nanostructures during thermally induced self-assembling on Ge(001) surface, Sci. Rep. **7**, 42420 (2017).

[52] E. Gnecco, R. Bennewitz, T. Gyalog, C. Loppacher, M. Bammerlin, E. Meyer, and H. J. Güntherodt, Velocity Dependence of Atomic Friction, Phys. Rev. Lett. **84**, 1172 (2000).

[53] Y. Sang, M. Dube, and M. Grant, Thermal Effects on Atomic Friction, Phys. Rev. Lett. **87**, 174301 (2001).

[54] L. Jansen, H. Hölscher, H. Fuchs, and A. Schirmeisen, Temperature Dependence of Atomic-Scale Stick-Slip Friction, Phys. Rev. Lett. **104**, 256101 (2010).

[55] E. Riedo, E. Gnecco, R. Bennewitz, E. Meyer, and H. Brune, Interaction Potential and Hopping Dynamics Governing Sliding Friction, Phys. Rev. Lett. **91**, 084502 (2003).

[56] C. M. Mate, G. M. McClelland, R. Erlandsson, and S. Chiang, Atomic-Scale Friction of a Tungsten Tip on a Graphite Surface, Phys. Rev. Lett. **59**, 1942 (1987).

[57] J. Luo and X. Zhou, Superlubricitive engineering—Future industry nearly getting rid of wear and frictional energy consumption, Friction **8**, 643 (2020).

[58] H. Wang and Y. Liu, Superlubricity achieved with two-dimensional nano-additives to liquid lubricants, Friction **8**, 1007 (2020).

[59] K. C. Mutyala, G. L. Doll, J. Wen, and A. V. Sumant, Superlubricity in rolling/sliding contacts, Appl. Phys. Lett. **115**, 103103 (2019).

[60] P. G. Grützmacher, S. Suarez, A. Tolosa, C. Gachot, G. Song, B. Wang, V. Presser, F. Mücklich, B. Anasori, and A. Rosenkranz, Superior wear-resistance of Ti3C2Tx multilayer coatings, ACS Nano **15**, 8216 (2021).